physica status solidi pss a
www.pss-a.com

Impedance Characterization of Organic Light-Emitting Structures with Thermally Activated Delayed Fluorescence

Alexander V. Voitsekhovskii, Sergey N. Nesmelov, Stanislav M. Dzyadukh, Tatyana N. Kopylova, and Konstantin M. Degtyarenko*

The organic light-emitting device (OLED) structures based on layer (2,8-bis[*N*,*N*-di(4 methoxyphenyl)amino]dibenzothiophene-*S*,*S*-dioxide) with thermally activated delayed fluorescence (TADF) are created. The properties of TADF-based structures are studied by measuring the impedance under various conditions (100 Hz–2 MHz and 10–300 K). The features of the capacitance–voltage curves of the studied structures can be explained by the simultaneous injection of holes from the anode and electrons from the cathode. Cole–Cole plots are studied at various voltages and temperatures. It is shown that at forward bias voltages, the impedance is determined by single relaxation process and at low voltages by more than one process. An OLED equivalent circuit consisting of four serial capacitance–resistance (CR) chains (CR–CR–CR–CR) is proposed. Using this circuit allows us to achieve good agreement between the calculated and experimental frequency dependences of the impedance at various voltages. The different elements of the equivalent circuit are associated with different layers in a multilayer OLED structure. The dependences of the CR element values on the bias voltage are found, and the thicknesses of the corresponding layers are determined.

1. Introduction

In recent decades, the technology of organic light-emitting diodes (OLED) has been actively developed, which is associated with the prospects for the widespread use of such devices in the creation of high-resolution flexible displays and efficient large-area lighting sources.[1–3] The most important OLED characteristic is quantum efficiency, which depends on the mechanisms of conversion of electric current through the device into radiation of the required spectral range.[4,5] When using phosphorescent materials, radiation occurs upon the transition of triplet excitons to the ground state, and in the case of fluorescent materials, recombination, which is accompanied by radiation, occurs only upon the transition of the singlet exciton to the ground state.[6] The fraction of triplet excitons (75%) is much higher than the fraction of singlet excitons (25%); therefore, phosphorescent OLEDs have much higher quantum efficiency.[7] The widespread use of highly effective phosphorescent OLEDs is hindered by the high cost of noble metals (iridium, platinum, and others) necessary for their production, as well as their limited reserves. In addition, phosphorescent materials are less stable compared with fluorescent materials.[8]

About 10 years ago, it was proposed to use thermally activated delayed fluorescence (TADF) for OLED, in which the excitation from the triplet channel is borrowed.[9] This mechanism is implemented in systems with a thermally approachable gap between the lowest triplet and singlet excited states. This makes it possible to significantly increase the efficiency of fluorescent OLED due to the use of both singlet and triplet excitons during electrical excitation.[10–12] Despite the large number of publications in this field, the search for materials with TADF is ongoing, and studies of the properties of TADF materials and OLED based on them are relevant.

Impedance (or admittance) measurements are a convenient and reliable method for studying the electrical characteristics of materials and device structures which is promising for use in OLED.[13–16] Based on the data of impedance spectroscopy, it is possible to construct equivalent schemes[17–20] that provide new information on the mechanisms of formation of the properties of organic devices.

In this work, a multilayer OLED structure based on the emission layer with TADF was created. As the emission layer, we used the material 2,8-bis[*N*,*N*-di(4 methoxyphenyl)amino] dibenzothiophene-*S*,*S*-dioxide, the photophysical properties of which were studied.[21] The electrical properties of TADF-based OLED structures have been investigated in detail by measuring impedance under various conditions.

2. Experimental Section

For the study, device OLED structures (indium tin oxide [ITO]/poly(3,4-ethylenedioxythiophene) polystyrene sulfonate [PEDOT:PSS]/2,2′-dimethyl-*N*,*N*′-di-[(1-naphthyl)-*N*,*N*′-diphenyl]-1,1′-biphenyl-4,4′-diamine [α-NPD]/TADF-layer/bathocuproine

Prof. A. V. Voitsekhovskii, Dr. S. N. Nesmelov, Dr. S. M. Dzyadukh, Prof. T. N. Kopylova, Dr. K. M. Degtyarenko
Nanoelectronics and Nanophotonics Laboratory and Laboratory for Organic Electronics
National Research Tomsk State University
36 Lenin av., Tomsk 634050, Russia
E-mail: nesm69@mail.ru

The ORCID identification number(s) for the author(s) of this article can be found under https://doi.org/10.1002/pssa.201900847.

DOI: 10.1002/pssa.201900847

[BCP]/LiF/Al) with an emission layer of 2.8-bis[*N*,*N*-di(4 methoxyphenyl)amino]dibenzothiophene-*S*,*S*-dioxide (TADF layer) were created. A layer of ITO was used as the anode, and 30 nm-thick PEDOT:PSS layer was deposited by centrifugation for hole injection.[22] A hole-transport layer with the thickness of 20 nm was formed from α-NPD. The emission TADF layer had the thickness of 50 nm. For the used TADF material, small gap was realized between the lower singlet level and the triplet level (<0.3 eV), which provides the possibility of the transition of excitons from the triplet to the singlet state with subsequent participation in electroluminescence. About 15 nm-thick BCP layer served as electron-transport and hall-blocking layers. Organic layers were formed by vacuum thermal deposition from quartz crucible (pressure 10^{-5} mbar, crucible temperature about 160 °C, deposition rate 0.02 nm s^{-1}). The properties of the deposited organic films were investigated using the ellipsometry method. Technological modes were optimized based on the results of a study of the spectral and electroluminescent properties of the fabricated OLED structures. The good electroluminescent characteristics of OLED structures[21] indicated the high quality of the deposited organic films. To form the cathode, 100 nm-thick aluminum layer and 1 nm-thick LiF layer were deposited. Vacuum thermal evaporation of LiF was conducted from a tantalum boat by heating LiF powder at the deposition rate of 0.1 A s^{-1}. Vacuum thermal evaporation of Al was conducted by heating a tungsten wire with a weight of Al at a deposition rate of 2 A s^{-1}. The distance from the sources to the substrate was 9 cm. The thicknesses of the deposited layers were monitored by a SQM 160 quartz meter, graduated from test sputtering, followed by measurement of the layer thicknesses on a Micro Xam 100 profilometer. At the end of the technological process, the capsulation of manufactured device structures was conducted, whose area was about 7 mm^2. The schematic representation of the layers in the test samples is shown in **Figure 1**a, and the schematic energy diagram of the OLED structure is shown in Figure 1b.

Impedance and current–voltage characteristics were measured using the setup based on Agilent E4980A immitance meter, LakeShore digital temperature controller, and Janis non-optical cryostat. The automated setup designed for admittance (impedance) spectroscopy of nanoheterostructures made it possible to make measurements at different frequencies (in the range from 100 Hz to 2 MHz) and temperatures (in the range from 9 to 300 K).

3. Results and Discussion

Figure 2a shows the dependences of current (I) and luminance (L) on the bias voltage for the fabricated TADF-based OLED

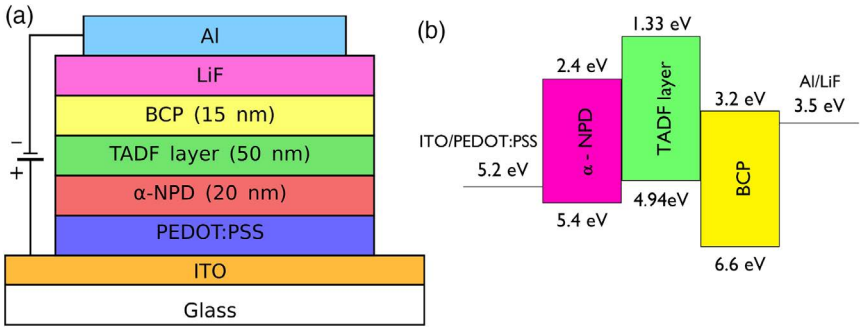

Figure 1. a) Schematic representation of the TADF-based OLED structure and b) schematic energy levels of TADF-based OLED structure.

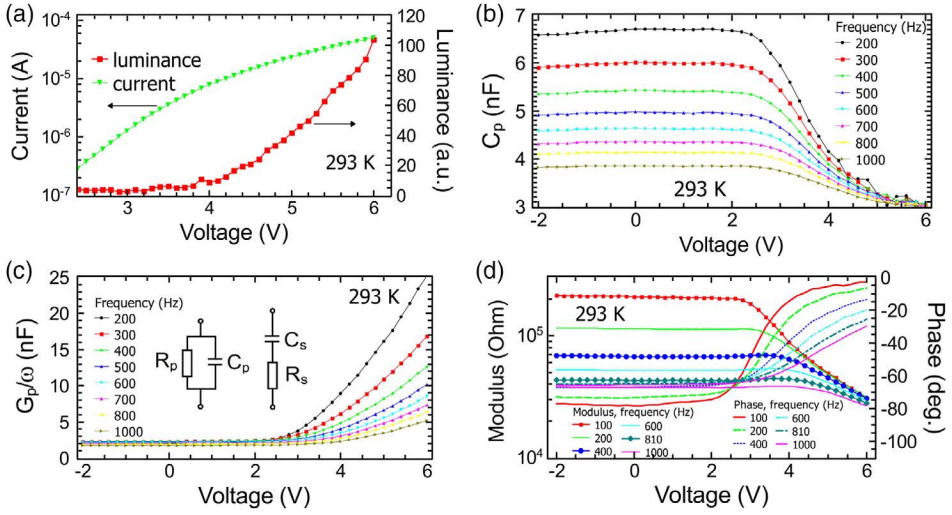

Figure 2. a) *I*–*V* and *L*–*V*, b) C_p–*V*, c) G_p/ω–*V*, and d) *Z*–*V* and φ–*V* dependences of the TADF-based OLED structure measured at the temperature of 293 K and (b,c) different frequencies.

structure, measured at the temperature of 293 K. It can be seen that a noticeable increase in the luminance occurs at forward voltages exceeding 3 V. The luminance at the voltage of 6 V decreases by about five times when the OLED structure is cooled to 260 K, which may be due to a decrease in the probability of the transition between triplet and singlet states. A decrease in this probability with cooling leads to a decrease in the contribution of excitons formed in the triplet state to the total electroluminescence luminance. Figure 2b,c shows the capacitance–voltage characteristics (C_p–V) and normalized conductance versus voltage (G_p/ω–V) for OLED structures measured at different frequencies. Parallel and serial equivalent circuits are shown in the inset in Figure 2c. Figure 2b shows that the luminescence region of the OLED structure corresponds to the capacitance reduction section. For the fabricated structure, in the frequency range 0.1–2000 kHz, there is no region of increase in capacitance at small forward biases.[23,24] This capacitance rise is usually associated with an increase in the amount of charge in the emission layer due to the injection of single type of charge carriers (e.g., hole injection from the anode).[24] In addition, the decrease in the capacitance due to the recombination of electrons and holes begins at relatively small forward biases. These features of the capacitance–voltage characteristics can be explained by the simultaneous injection of holes from the anode and electrons from the cathode, which is possible with a low-work-function material as the cathode. In this case, OLED structures are double carrier devices. For the structure, a strong dependence of the form of the capacitance–voltage characteristics on the frequency is observed.[25] The conductance of the structure increases at bias voltages exceeding 3 V.

The results of measuring admittance with a parallel equivalent circuit (C_p, $R_p = 1/G_p$) can be converted into capacitance and resistance with a sequential circuit (C_s, R_s) using the relations

$$C_s = \frac{1+\omega^2 C_p^2 R_p^2}{\omega^2 C_p R_p^2},\ R_s = \frac{R_p}{1+\omega^2 C_p^2 R_p^2} \tag{1}$$

where ω is the angular frequency, $\omega = 2\pi F$, and F is the frequency in hertz.

The impedance Z of such an R_s–C_s chain can be written as

$$\begin{aligned} Z(\omega) &= \mathrm{Re}\, Z + j\,\mathrm{Im}\, Z = R_s - j\frac{1}{\omega C_s} \\ &= \frac{R_p}{1+\omega^2 C_p^2 R_p^2} - j\frac{\omega C_p R_p^2}{1+\omega^2 C_p^2 R_p^2} \end{aligned} \tag{2}$$

where Re Z is the real part of the impedance, and Im Z is the imaginary part of the impedance.

The impedance module and phase (φ) can be written as

$$|Z| = \sqrt{(\mathrm{Re}\, Z)^2 + (\mathrm{Im}\, Z)^2},\ \phi = \mathrm{arctg}\left(\frac{\mathrm{Im}\, Z}{\mathrm{Re}\, Z}\right) \tag{3}$$

Figure 2d shows the dependences of the impedance modulus and phase on voltage measured at different frequencies. The impedance modulus was calculated from experimental Re Z and Im Z dependences using Equation (3). Figure 2d shows that the impedance modulus decreases at voltages exceeding 3 V. In the range of bias voltages from −2 to 3 V, the capacitive component of the impedance dominates, but at large forward biases, the phase tends to zero. The region of decrease in the impedance modulus corresponds to the transition of the OLED structure from the insulating state to conducting state. The observed form of the frequency dependence of the impedance modulus and phase is typical for OLED structures.[15] The frequency dependence of the phase in the insulating state is associated with the use of sufficiently high (for the fabricated structure) frequencies for measurements.

Figure 3a shows the experimental dependences of –Im Z on Re Z for TADF-based OLED structures (Cole–Cole plots),[26–29] measured at the temperature of 300 K and various bias voltages. To describe the ideal Cole–Cole plots in the presence of a single relaxation process, the simple equivalent circuit shown in the inset in Figure 3a is often used. In this case, we can write the relation[29]

$$\left[\mathrm{Re}\, Z - \left(R_s - \frac{R_p}{2}\right)\right]^2 + [\mathrm{Im}\, Z]^2 = \frac{R_p^2}{4} \tag{4}$$

Equation (4) defines a circle centered at the point $(R_s + \frac{1}{2}R_p; 0)$ with a diameter equal to R_p.[30] Figure 3a shows that for the studied structure, the Cole–Cole plots are close to the semicircle at the voltages of 5 and 6 V. When viewed accurately, the semicircle is slightly depressed, but this feature is very poorly expressed. Therefore, in a first approximation, we can consider an equivalent circuit containing capacitors, rather than constant phase elements. The Cole–Cole plots have a more complex shape in the voltage range from 0 to 3 V. This indicates that to describe the processes in the OLED structures in the insulating state, it is necessary to use a more complex equivalent circuit with several relaxation times. Figure 3b shows Cole–Cole plots at 6 V and various temperatures. The Cole–Cole plots retain a shape close to the perfect semicircle when the temperature decreases, but their radius increases with cooling. According to Equation (4), an increase in the semicircle radius is associated with an increase in the resistance value R_p with a decreasing temperature (inset in Figure 3a). Figure 3c shows Cole–Cole plots at the voltages of 0 and 6 V plotted in logarithmic axes. It is known that the slope of the approximating straight line to the perfect semicircle in the log–log representation is 0.5, which is often used in the analysis of the Cole–Cole plots.[31,32] The experimental data at the voltage of 6 V are in good agreement with linear approximation, and the slope of the straight line is 0.513, which is close to 0.5. This means that the Cole–Cole plots for the OLED structure under study at large forward biases are very close to the perfect semicircle, which is possible if single relaxation process dominates. At zero voltage and high frequencies, the slope of the approximating straight line somewhat increased (up to 0.564). At the low frequencies, there is a significant deviation of the Cole–Cole plot from the semicircle. This is due to the fact that at low frequencies and small positive biases, the impedance is determined by several relaxation processes. Figure 3d shows that the R_p–V dependence is a straight line with the slope $m = -2.45$ when using the logarithmic axes. This indicates that a space-charge limited current with exponential trap distribution is realized in the OLED structure.[29,32,33] The resistance R_p, shown in Figure 3b, increases almost by four times with cooling from 300 to 200 K.

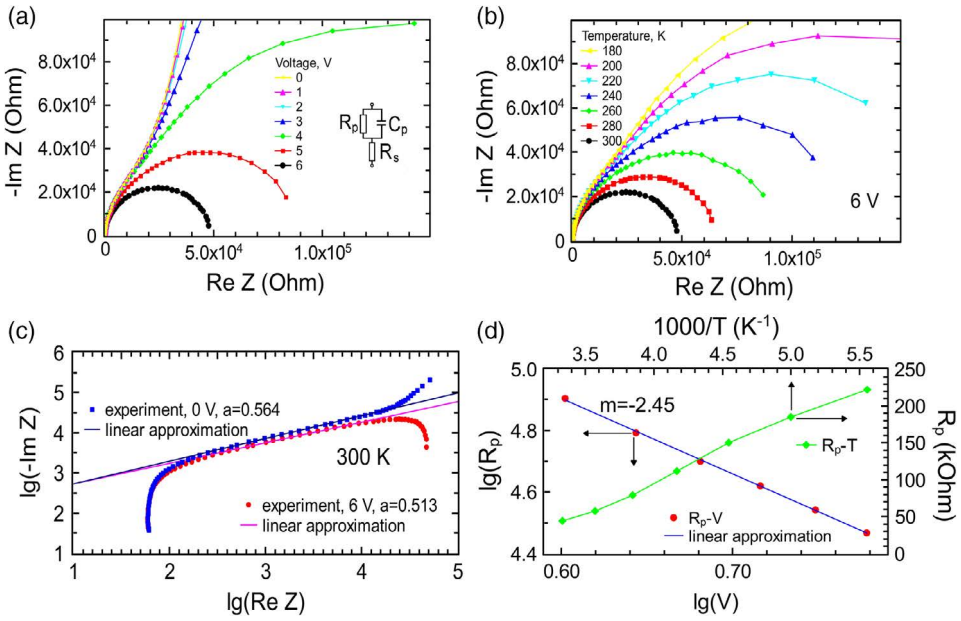

Figure 3. a) Measured Cole–Cole plots with variation of the voltage at the temperature of 300 K, b) Cole–Cole plots with variation of the temperature at the voltage of 6 V, c) Cole–Cole plots for OLED structure at 6 V and 300 K (in log–log representation), and d) dependences of resistance R_p on voltage (in log–log representation) at the temperature of 300 K and on temperature at the voltage of 6 V.

The fitting of equivalent circuit parameters to the frequency impedance dependences provides more detailed information about the properties of structures than just an analysis of Cole–Cole plots. To select the equivalent circuit of the OLED structure and determine the values of its elements, we used a comparison of the experimental frequency dependences of Re Z and Im Z with the fitting results obtained using the equivalent circuit method (**Figure 4**a,b). Good agreement between the experimental and calculated dependences can be achieved using four serial capacitance–resistance (CR) chains as an equivalent circuit (CR–CR–CR–CR chain, inset in Figure 4a). In this equivalent circuit, C_4 and R_4 are capacitance and resistance for series CR chain,[33,34] the values of which are practically independent of voltage and temperature ($C_4 \approx 150$ pF, $R_4 \approx 61\ \Omega$). To determine the values of the elements of the equivalent circuit (inset in Figure 4a), the calculated frequency dependences of the impedance were fitted to the experimental dependences. The values of the elements of the equivalent circuit of the OLED structure, determined at different voltages, are shown in **Table 1**.

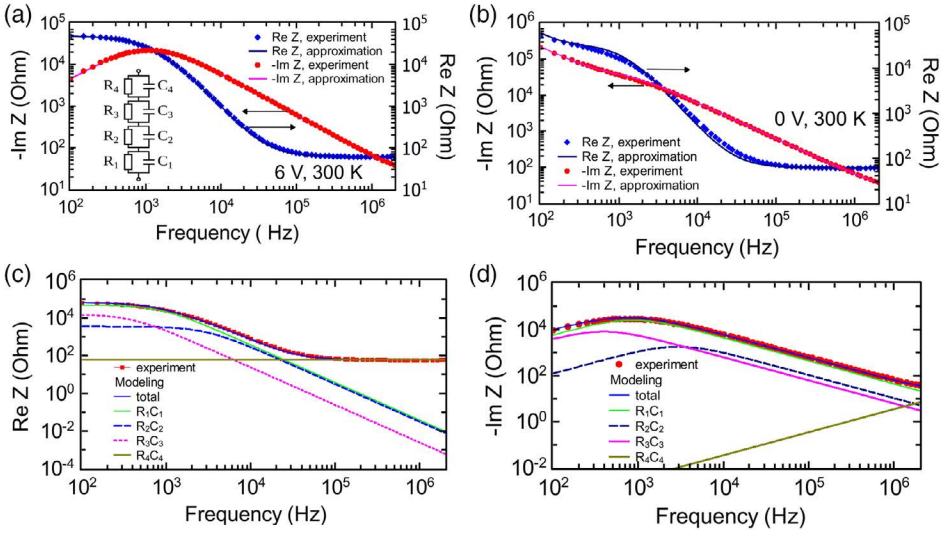

Figure 4. a) Experimental and calculated Re Z–F and –Im Z–F dependences for the TADF-based OLED structure at the bias voltage of 6 V and b) at the bias voltage of 0 V. c) Experimental and calculated frequency dependences of the components Re Z and d) –Im Z at the voltage of 6 V and the temperature of 280 K.

Table 1. Parameters of the equivalent circuit of the OLED structure at different voltages and temperature of 300 K.

Voltage [V]	C_1 [nF]	R_1 [kΩ]	C_2 [nF]	R_2 [kΩ]	C_3 [nF]	R_3 [kΩ]
0	8.9	1512	4.0	33	53	391
1	8.8	1396	4.0	31	53	369
2	8.6	1128	4.1	28	52	297
3	8.2	428	4.1	26	39	171
4	7.6	148	4.3	20	32	51
5	5.6	74	6.3	10	25	17
6	3.8	33	15.1	3	22	12

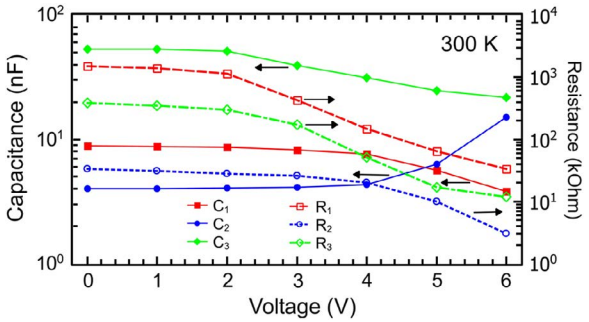

Figure 5. Dependences of the values of the equivalent circuit elements on the bias voltage.

Figure 4c,d shows the experimental frequency dependences of the impedance of the OLED structure at the temperature of 280 K and the voltage of 6 V, as well as the calculated dependences Re Z and Im Z for a full equivalent circuit and for individual parallel CR chains. For Re Z and Im Z of the full equivalent circuit of the OLED structure, considering Equation (1) and (2), we can write the following expression

$$\mathrm{Re}\,Z = \sum_{k=1}^{4} \mathrm{Re}\,Z_k = \sum_{k=1}^{4} \frac{R_{pk}}{1+\omega^2 C_{pk}^2 R_{pk}^2},\ \mathrm{Im}\,Z = -\sum_{k=1}^{4} \mathrm{Im}\,Z_k = \sum_{k=1}^{4} \frac{\omega C_{pk} R_{pk}^2}{1+\omega^2 C_{pk}^2 R_{pk}^2} \quad (5)$$

where C_{pk} and R_{pk} are the parallel capacitance and resistance of the chain with number k. Modeling using Equation (5) showed that it is easy to determine the values of R_4 and C_4 from impedance measurements at high frequencies. The values of R_2 and C_2 have a significant effect on the impedance at medium frequencies (10–100 kHz), and the values of R_3 and C_3 affect the impedance at low frequencies (0.1–10 kHz). The values of R_1 and C_1 determine the impedance in a wide range of frequencies (so Im Z significantly depends on C_1 at $F < 1$ MHz). Therefore, the values of R_1 and C_1 can be found with the greatest accuracy. Note that the maximum in the frequency dependence of the imaginary part of the impedance is determined by the dominant CR chain, which should be considered when extending the method for determining mobility to multilayer structures.[35]

Figure 5 shows the dependences of the values of the elements of the equivalent circuit on the bias voltage at the temperature of 300 K. All resistances (except R_4) significantly decrease with increase in the positive bias voltage and the transition of the OLED structure to the conducting state. Capacitances C_1 and C_3 decrease with increase in positive voltage on the structure, and capacitance C_2 increases. By analyzing the voltage dependences of the elements of the equivalent circuit, various CR chains are associated with different regions in the OLED structure. These regions are not uniquely associated with layers of various materials, but differ in electrical properties (e.g., these are depleted and conducting regions).[36,37] The following physical meaning of the elements of the equivalent circuit is possible. Capacitance C_2 and resistance R_2 are associated with the quasi-neutral bulk of the emission layer, which has a relatively high conductivity. The chains R_1–C_1 and R_3–C_3 characterize the properties of the depletion layers at the cathode and anode, respectively. Capacitance C_4 and resistance R_4 reflect the properties of the contacts. Elements R_1 and C_1 characterize the space charge region (SCR), which propagates from the cathode. This SCR captures the electron-transport layer (BCP) and penetrates into the TADF layer. To describe the elements of the equivalent circuit, we used for a capacitor the model of two flat plates. This approach is often used,[36] but it is an approximation, as it assumes interface flatness and layer homogeneity. Within this approximation, the capacitance C_1 can be described by the expression: $C_1 = \frac{\epsilon\epsilon_0 S}{d_1}$, where ϵ_0 is the dielectric constant of vacuum, ϵ is the relative dielectric constant of organic semiconductor, S is the structure area, and d_1 is the thickness of the depleted layer. If we assume that for organic semiconductors $\epsilon = 3$,[36] then the thickness d_1 is 20.9 and 48.9 nm at 0 and 6 V, respectively. The values of R_2 and C_2 characterize the properties of the bulk of the emission TADF layer. The thickness of this layer d_2 is 46.5 and 12.3 nm at 0 and 6 V, respectively. The values of the elements R_3 and C_3 characterize the SCR at the anode. The thickness of this layer (d_3) is 3.5 and 8.4 nm at 0 and 6 V, respectively. The total layer thickness ($d_1 + d_2 + d_3$) is 70.9 and 69.6 nm at 0 and 6 V, respectively, which is quite close to the sum of the thicknesses of the TADF layer and the BCP layer. The α-NPD-transport layer does not significantly affect the measured impedance due to its low resistance. The experimental results obtained are in good agreement with the results of numerical simulations of the impedance and admittance of the OLED structure (ITO/α-NPD/Alq3/LiF-Al).[36]

4. Conclusions

Thus, device OLED structures with a TADF emission layer were fabricated. The electrical characteristics of TADF-based OLED structures are investigated using impedance measurements at various voltages, frequencies, and temperatures. From the capacitance–voltage characteristics, it follows that the samples studied are double carrier devices. It follows from the Cole–Cole plots that single relaxation process dominates in the impedance formation in the conducting state of the structure and two or more relaxation processes dominate in the insulating state. At positive bias voltages, a space-charge limited current flows through the OLED structure. To explain the frequency dependences of Re Z and –Im Z, numerical modeling was conducted,

which showed that the explanation of the experimental results is possible using the CR–CR–CR–CR equivalent circuit. Parallel CR chains can characterize the SCRs from the side of the anode and cathode, as well as the bulk of the emission TADF layer. The dependences of the values of the equivalent circuit elements on the bias voltage are found, and the thicknesses of the layers at various biases are determined. It is shown that the total layer resistance in the OLED structure decreases with cooling. A more complete characterization of the TADF-based OLED structure requires impedance measurements at lower frequencies or higher temperatures.

Acknowledgements

This study was supported by the Russian Foundation for Basic Research and the Administration of the Tomsk region as part of a research project no. 18-43-700005.

Conflict of Interest

The authors declare no conflict of interest.

Keywords

Cole–Cole plots, impedance spectroscopy, organic light-emitting devices, organic semiconductors, thermally activated delayed fluorescence

Received: October 7, 2019
Revised: December 20, 2019
Published online: January 24, 2020

[1] *Organic Light-Emitting Diodes (OLEDs): Materials, Devices and Applications* (Ed: A. Buckley), Elsevier, Amsterdam/New York **2013**.
[2] C. Branas, F. J. Azcondo, J. M. Alonso, *IEEE Ind. Electron. Mag.* **2013**, *7*, 6.
[3] J. Wang, F. Zhang, J. Zhang, W. Tang, A. Tang, H. Peng, Z. Xu, F. Teng, Y. Wang, *J. Photochem. Photobiol. C* **2013**, *17*, 69.
[4] G. Gu, D. Z. Garbuzov, P. E. Burrows, S. Venkatesh, S. R. Forrest, M. E. Thompson, *Opt. Lett.* **1997**, *22*, 396.
[5] M. Furno, R. Meerheim, S. Hofmann, B. Lüssem, K. Leo, *Phys. Rev. B* **2012**, *85*, 115205.
[6] S. Kappaun, C. Slugovc, E. List, *Int. J. Mol. Sci.* **2008**, *9*, 1527.
[7] C. Adachi, M. A. Baldo, M. E. Thompson, S. R. Forrest, *J. Appl. Phys.* **2001**, *90*, 5048.
[8] Q. Zhang, B. Li, S. Huang, H. Nomura, H. Tanaka, C. Adachi, *Nat. Photonics* **2014**, *8*, 326.
[9] A. Endo, M. Ogasawara, A. Takahashi, D. Yokoyama, Y. Kato, C. Adachi, *Adv. Mater.* **2009**, *21*, 4802.
[10] V. Jankus, P. Data, D. Graves, C. McGuinness, J. Santos, M. R. Bryce, F. B. Dias, A. P. Monkman, *Adv. Funct. Mater.* **2014**, *24*, 6178.
[11] D. J. Volz, *J. Photonics Energy* **2016**, *6*, 020901.
[12] F. B. Dias, K. N. Bourdakos, V. Jankus, K. C. Moss, K. T. Kamtekar, V. Bhalla, J. Santos, M. R. Bryce, A. P. Monkman, *Adv. Mater.* **2013**, *25*, 3707.
[13] C. K. Suman, J. Yun, S. Kim, S. D. Lee, C. Lee, *Curr. Appl. Phys.* **2009**, *9*, 978.
[14] C. T. Tsai, Y. Y. Chen, P. C. Kao, S. Y. Chu, *Solid-State Electron.* **2019**, *158*, 85.
[15] X. W. Zhang, J. W. Xu, H. R. Xu, H. Wang, C. L. Xie, B. Wei, X. Y. Jiang, Z. L. Zhang, *J. Phys. D: Appl. Phys.* **2012**, *46*, 055102.
[16] J. M. Kim, J. J. Kim, *Org. Electron.* **2019**, *67*, 43.
[17] L. S. C. Pingree, B. J. Scott, M. T. Russell, T. J. Marks, M. C. Hersam, *Appl. Phys. Lett.* **2005**, *86*, 073509.
[18] A. Pitarch, K. Meerholz, D. Hertel, *Phys. Status. Solidi B* **2008**, *245*, 814.
[19] M. Radaoui, A. B. Fredj, S. Romdhane, D. A. M. Egbe, N. S. Sariciftci, H. Bouchriha, *Synth. Met.* **2015**, *210*, 352.
[20] Y. Guo, W. Wang, S. Li, Y. Liu, T. Liu, Q. Wang, Q. Wang, X. Gao, Q. Fan, W. Li, *Solid-State Electron.* **2019**, *153*, 46.
[21] R. M. Gadirov, R. R. Valiev, L. G. Samsonova, K. M. Degtyarenko, N. V. Izmailova, A. V. Odod, S. S. Krasnikova, I. K. Yakuschenko, T. N. Kopylova, *Chem. Phys. Lett.* **2019**, *717*, 53.
[22] A. V. Voitsekhovskii, S. N. Nesmelov, S. M. Dzyadukh, T. N. Kopylova, K. M. Degtyarenko, A. P. Kokhanenko, *Russ. Phys. J.* **2019**, *62*, 306.
[23] I. H. Campbell, D. L. Smith, J. P. Ferraris, *Appl. Phys. Lett.* **1995**, *66*, 3030.
[24] V. Shrotriya, Y. J. Yang, *J. Appl. Phys.* **2005**, *97*, 054504.
[25] M. Meier, S. Karg, W. J. Riess, *J. Appl. Phys.* **1997**, *82*, 1961.
[26] K. S. Cole, H. S. Cole, *J. Chem. Phys.* **1942**, *9*, 341.
[27] X. Zhang, B. Mo, F. You, X. Zhou, L. Liu, H. Wang, *Optik* **2016**, *127*, 1424.
[28] R. V. Rajan, S. Gowri, N. Manopradha, D. R. Leenaraj, L. K. Joy, D. Sajan, *Opt. Laser Technol.* **2019**, *119*, 105664.
[29] H. Hrichi, K. Hriz, M. Benzarti-Ghédira, N. Jaballah, R. B. Chaâbane, M. Majdoub, H. B. Ouada, *Mater. Sci. Semicond. Process.* **2013**, *16*, 851.
[30] J. R. Macdonald, *Impedance Spectroscopy-Emphasizing Solid Materials and Systems*, Wiley-Interscience, John Wiley and Sons, New York **1987**.
[31] A. K. Jonscher, *Dielectric Relaxation in Solids*, Dielectrics Pub., London, UK **1983**.
[32] S. H. Kim, K. H. Choi, H. M. Lee, D. H. Hwang, L. M. Do, *J. Appl. Phys.* **2000**, *87*, 882.
[33] A. J. Campbell, D. D. C. Bradley, D. G. Lidzey, *J. Appl. Phys.* **1997**, *82*, 6326.
[34] V. S. Reddy, S. Das, S. K. Ray, A. Dhar, *J. Phys. D: Appl. Phys.* **2007**, *40*, 7687.
[35] D. C. Tripathi, A. K. Tripathi, Y. N. Mohapatra, *Appl. Phys. Lett.* **2011**, *98*, 14.
[36] N. D. Nguyen, M. Schmeits, *Phys. Status Solidi A* **2006**, *203*, 1901.
[37] J. Scherbel, P. H. Nguyen, G. Paasch, W. Brütting, M. Schwoerer, *J. Appl. Phys.* **1998**, *83*, 5045.